

# Observation of an inverse turbulent-wave cascade in a driven quantum gas

Andrey Karailiev,<sup>1</sup> Martin Gazo,<sup>1</sup> Maciej Gałka,<sup>1,2</sup> Christoph Eigen,<sup>1</sup> Tanish Satoor,<sup>1</sup> and Zoran Hadzibabic<sup>1</sup>

<sup>1</sup>*Cavendish Laboratory, University of Cambridge, J. J. Thomson Avenue, Cambridge CB3 0HE, United Kingdom*

<sup>2</sup>*Physikalisches Institut der Universität Heidelberg, Im Neuenheimer Feld 226, 69120 Heidelberg, Germany*

We observe an inverse turbulent-wave cascade, from small to large lengthscales, in a homogeneous 2D Bose gas driven isotropically on a lengthscales much smaller than its size. Starting with an equilibrium condensed gas, at long drive times we observe a nonthermal steady state. At increasing lengthscales, starting from the forcing one, the steady-state momentum distribution features in turn: (i) a power-law spectrum, with an exponent close to the analytical result for a particle cascade in weak-wave turbulence, and (ii) a spectrum intriguingly reminiscent of a nonthermal fixed point associated with universal coarsening in an isolated 2D gas. In further experiments, based on anisotropic driving, we also reveal the qualitative picture of the cascade-formation dynamics.

Richardson's direct cascade [1–3], which transports excitations from large to small lengthscales, provides a canonical picture of turbulence and underpins its modern understanding in systems ranging from interplanetary plasmas to financial markets [4, 5]. However, depending on the transport-conserved quantities, turbulence can also feature inverse cascades [6], from small to large lengthscales (see Fig. 1). For vortex-dominated turbulence, inverse cascades are seen [7–12], for example, in Jupiter's atmosphere [9] and Onsager's vortex clustering [10–12]. For wave turbulence, they have been predicted for systems including gravitational waves in the early universe [13, 14] and magnetized plasmas in neutron stars [15, 16]. Experimentally, evidence for inverse wave cascades has been observed in decaying one-dimensional (1D) turbulence in nonlinear optics [17–19] and for driven surface waves on water [20].

In this Letter we realize and study an inverse turbulent-wave cascade in a homogeneous 2D Bose gas [21, 22], by continuously driving it on a lengthscales much smaller than its size. Starting with an equilibrium condensate and isotropically exciting particles to a large wavenumber  $k_F$ , at long times we observe a stationary nonthermal momentum distribution  $n_k$ . For wavenumbers  $k_\xi \lesssim k \lesssim k_F$ , where  $1/k_\xi$  is the healing length of the initial condensate, we observe a power-law spectrum  $n_k \propto k^{-\gamma}$ , with  $\gamma = 1.55(15)$ , close to the analytical result  $\gamma = 4/3$  for a particle cascade in weak-wave turbulence (WWT) [23]. At lower  $k$  this behavior breaks down, but  $n_k$  also differs from that of the equilibrium condensate; intriguingly, it shows similarity to the spectrum associated with a nonthermal fixed point (NTFP) [24] that characterizes coarsening in an isolated 2D Bose gas [25, 26]. We also show that the salient features of the cascade survive for anisotropic (uniaxial) driving, and study the dynamics of the steady-state formation, observing qualitative agreement with theory [27–30].

We start with a 2D quasi-pure  $^{39}\text{K}$  condensate of  $5 \times 10^4$  atoms in the lowest hyperfine state, confined in the  $x$ - $y$  plane by a circular optical box trap of radius  $R = 22 \mu\text{m}$  and depth  $U_D = k_B \times 150 \text{ nK}$ ; the gas is confined to the plane by a harmonic trap with frequency  $\omega_z/(2\pi) = 1.5 \text{ kHz}$  [31]. We set the  $s$ -wave scattering length  $a$  to  $30 a_0$  (where  $a_0$  is the Bohr radius) using the 402.7-G Feshbach resonance [32], so the dimensionless interaction parameter is  $\tilde{g} = a\sqrt{8\pi m\omega_z/\hbar} = 0.02$

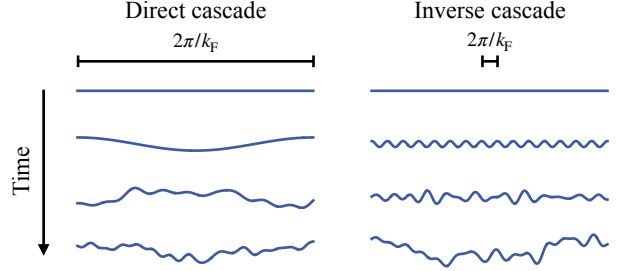


FIG. 1. Real-space cartoons of direct and inverse cascades. The direct cascade corresponds to the transport of excitations from large to small lengthscales (small to large wavenumbers), and the inverse one to transport from small to large lengthscales. Here  $k_F$  is the wavenumber at which the energy is continuously injected, starting at time  $t = 0$ . For wave turbulence in a Bose gas, the direct cascade with an idealized sink (dissipation) at  $k/k_F \rightarrow \infty$  corresponds to a scale-invariant energy flux in momentum space, without any particle flux. Similarly, the inverse cascade with a sink at  $k/k_F \rightarrow 0$  corresponds to a pure particle flux, without any energy flux.

(where  $m$  is the atom mass) [33]. The particle density is  $n = 33 \mu\text{m}^{-2}$ , the inverse healing length is  $k_\xi = \sqrt{\tilde{g}n} \approx 0.8 \mu\text{m}^{-1}$ , and the trap depth sets the high- $k$  dissipation scale,  $k_D = \sqrt{2mU_D/\hbar} \approx 5 \mu\text{m}^{-1}$  [34]. We use matter-wave focusing [26, 35] to measure the 2D momentum distributions  $n_k$ , which we normalize so that  $\int n_k d^2\mathbf{k} = 1$ .

As in theoretical studies [23, 36–38], we drive the system isotropically at  $|\mathbf{k}| = k_F \gg 1/R$ ; however, note that theorists typically consider particles injected into an initially empty system, whereas the particles we inject at  $k_F$  initially come from the condensate and are at later times recirculated from the low- $k$  states. As illustrated in Fig. 2(a), we use a digital micromirror device (DMD) to project onto the atomic cloud a grayscaled [39, 40] radially symmetric time-varying potential,  $U(r, t) = f(r) \sin(\omega t)$ , where  $f(r)$  mimics the spatial structure of the excited mode [41]. The approximate radial period of  $f(r)$  is  $3.0 \mu\text{m}$ , corresponding to  $k_F = 2.1 \mu\text{m}^{-1}$ , and our drive frequency,  $\omega/(2\pi) = 710 \text{ Hz}$ , matches the Bogoliubov-dispersion  $\omega(k_F)$  [42].

At long drive times,  $\omega t/(2\pi) \geq 75$ , we observe a (quasi-) steady far-from-equilibrium  $n_k$ , such as shown in Fig. 2(b) for  $\omega t/(2\pi) = 200$ . As indicated by the arrows, our driving at  $k_F$

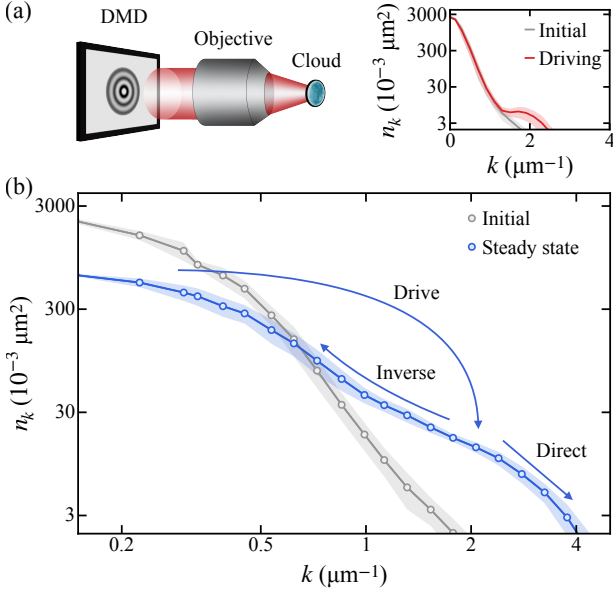


FIG. 2. Forcing and steady state. (a) Left: we drive our box-trapped atomic cloud of radius  $R = 22 \mu\text{m}$  isotropically at  $k_F \approx 2.1 \mu\text{m}^{-1} \gg 1/R$ , using a digital micromirror device (DMD) to create a temporally oscillating potential. Right: momentum distribution after two drive periods (red) shows excitations above the initial equilibrium state (gray). (b) Far-from-equilibrium steady state (blue), shown for  $\omega t/(2\pi) = 200$  and contrasted with the initial equilibrium distribution (gray). In both panels, the lines and points show azimuthally-averaged data, and the shading indicates azimuthal variations (standard deviation). From hereon (Figs. 3 and 4) we show just the azimuthal averages.

results in both inverse and direct cascades. Since our  $k_D$  is not infinite, the direct cascade carries a nonzero particle flux [34] and results in a slow reduction of the total atom number (by 30% between  $\omega t/(2\pi) = 75$  and 200), but we find that the normalized  $n_k$  remains essentially stationary. Here we focus on the inverse cascade, while the direct one was studied with low- $k_F$  driving in [43]; in that case  $n_k \propto k^{-2.9}$  was observed (indicated in Fig. 2(b) by the slope of the arrow).

In Fig. 3 we focus on the spectral range  $k_\xi \lesssim k \lesssim k_F$ , where the dispersion relation is particle-like. In Fig. 3(a) we show for four different drive times that the essentially stationary spectrum is power-law-like,  $n_k = n_0 (k/k_F)^{-\gamma}$ , with  $\gamma = 1.55(15)$ . Our  $\gamma$  is close to an analytical result  $\gamma = 4/3$ , for a particle cascade in WWT [23], but note that the validity of this solution to kinetic equations was questioned by the authors themselves (see also [18]). In Fig. 3(b) we show how this spectrum emerges in time, by plotting the evolution of  $n_0$  and  $\gamma$  obtained from power-law fits of  $n_k$ .

At lower  $k$ , this power-law behavior breaks down. Here, the initial condensate is replaced by a nonthermal distribution that is captured well by  $n_k \propto 1/(1 + (k/k_0)^\kappa)$ , with  $\kappa = 3$  (see Fig. 4). Interestingly, the same form of  $n_k$ , with the same  $\kappa$ , characterizes the particle flow to low  $k$  during coarsening in an isolated 2D Bose gas [25, 26], which is understood in terms of the system being attracted to an NTFP [24]. However,

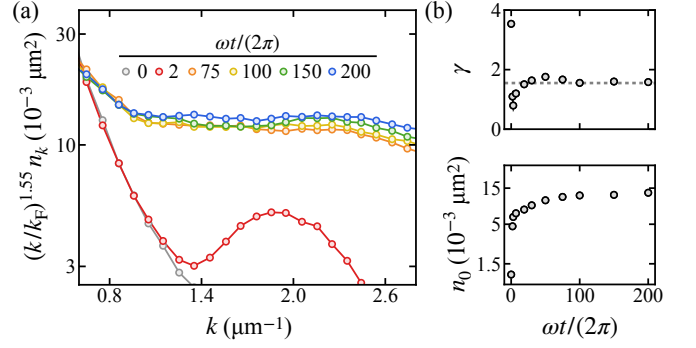


FIG. 3. Steady-state turbulent cascade for  $k_\xi \lesssim k \lesssim k_F$ . (a) The flatness of the compensated spectra,  $(k/k_F)^{1.55} n_k$ , shows that the nearly stationary long-time distributions are close to the power-law form  $n_k = n_0 (k/k_F)^{-\gamma}$ , with  $\gamma = 1.55$ . The analytical result for a particle cascade in WWT is  $\gamma = 4/3$ . (b) Cascade amplitude,  $n_0$ , and exponent,  $\gamma$ , extracted from power-law fits of  $n_k$  for  $k = 1.0\text{--}2.1 \mu\text{m}^{-1}$ ; note that the power-law fits are good only for  $\omega t/(2\pi) \geq 50$ . The dashed line shows  $\gamma = 1.55$ .

during coarsening  $k_0$  decreases algebraically in time, whereas here, under continuous driving, the excitations are recirculated in  $k$ -space and  $k_0$  is constant [44]. Tentatively, this can be interpreted as the system being stabilized near an NTFP.

We now turn to experiments where we change the driving potential to further study the cascade-formation dynamics. Here we drive the gas along only one direction,  $x$  [see Fig. 5(a)], and also switch to a square box trap (of side length  $30 \mu\text{m}$ ), while keeping  $n$ ,  $k_\xi$ , and  $k_F$  the same as in Figs. 2-4.

First, in Fig. 5(a) we show, for  $\omega t/(2\pi) = 2$ , that the injection of excitations into modes with wavevectors close to the  $x$  axis is similar to before [see Fig. 2(a)], but the modes with wavevectors close to the  $y$  axis are not directly excited by the drive. Here  $n_k^x(k)$  denotes populations averaged over  $\mathbf{k}$  vectors within  $\pi/8$  radians of the  $x$  axis (parallel to the drive), and

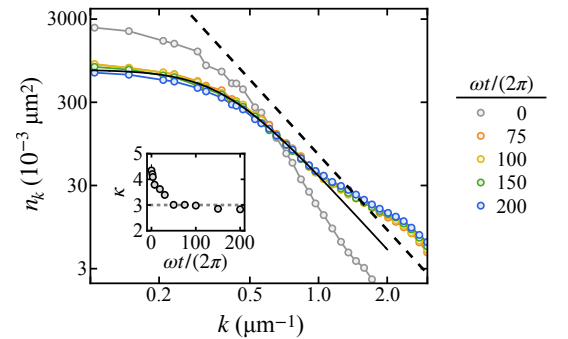


FIG. 4. Nonthermal  $n_k$  at  $k \lesssim k_\xi$ . At long times,  $n_k$  for  $k \leq 1 \mu\text{m}^{-1}$  is captured well by  $n_k \propto 1/(1 + (k/k_0)^\kappa)$  with  $\kappa = 3$  (solid black line; the dashed line shows  $n_k \propto k^{-3}$ ). The same form of  $n_k$ , with the same  $\kappa$ , characterizes coarsening in an isolated 2D Bose gas, but in that case  $k_0$  decreases algebraically in time, whereas here, under continuous driving, it remains constant ( $\approx 0.4 \mu\text{m}^{-1}$ ). The inset shows the evolution of  $\kappa$ , fitted as a free parameter.

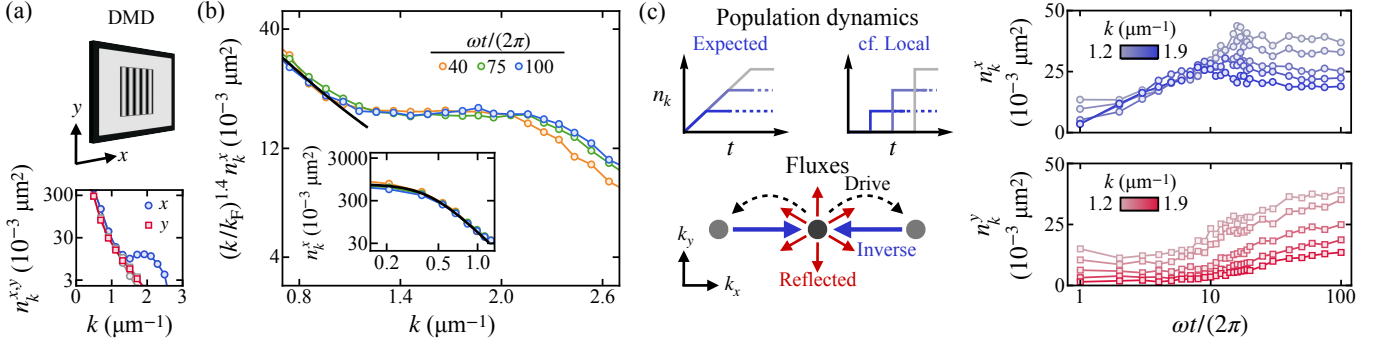


FIG. 5. Steady state and cascade-formation dynamics for anisotropic driving. (a) Here we use a square box trap and change the DMD pattern to drive the gas uniaxially, at  $(k_x, k_y) = (\pm k_F, 0)$ , with the same  $k_F$  as in Figs. 2-4. The bottom panel shows, for  $\omega t/(2\pi) = 2$  (in color; cf.  $t = 0$  in gray), that excitations are created along  $x$  and not along  $y$ . Here  $n_k^x(k)$  (resp.  $n_k^y(k)$ ) is the average population of modes with wavevectors within  $\pi/8$  radians of the  $x$  (resp.  $y$ ) axis. (b) Along  $x$  we observe essentially the same steady state as for the isotropic driving, with  $\gamma = 1.4(1)$  for  $k_\xi \lesssim k \lesssim k_F$  and  $\kappa = 3$  (black line in the main panel and inset) at lower  $k$ . (c) Population dynamics along  $x$  and  $y$ . The top cartoons show the expected non-local dynamics along the drive and, for comparison, what the dynamics would be if they were local; darker blue corresponds to higher  $k$ . The bottom cartoon shows the uniaxial drive to  $(\pm k_F, 0)$ , the inverse particle flux, and the reflected flux; for isotropic driving both fluxes are isotropic, while here we expect the inverse one to be uniaxial and the reflected one to be omnidirectional. Our  $n_k^x$  data (top panel) are consistent with the expected non-local dynamics, while the  $n_k^y$  data (bottom panel) reveal the delayed reflected flux.

$n_k^y(k)$  denotes populations of modes with wavevectors within  $\pi/8$  radians of the  $y$  axis (perpendicular to the drive).

Next, in Fig. 5(b) we show that along the drive direction the long-time behavior is essentially the same as for the isotropic drive, which implies that the cascade dynamics are azimuthally local: we observe a stationary power-law  $n_k^x$ , with  $\gamma = 1.4(1)$ , for  $k_\xi \lesssim k \lesssim k_F$ , while  $n_k^x$  at lower  $k$  is captured well by the same form as in Fig. 4, with  $\kappa = 3$ . Note that here the steady state is reached for  $\omega t/(2\pi) \approx 40$ .

Finally, in Fig. 5(c) we study the cascade formation by looking at the dynamics of both  $n_k^x$  and  $n_k^y$ ; the cartoons outline the two key theoretical concepts that our data support. First, for isotropic driving,  $n_k$  at different  $k$  are expected to initially grow in unison [27, 29], which means that the inverse cascade, in contrast to the direct one [43], is not local in  $k$ -space (see top cartoons). Here, this expectation should apply (only) to the dynamics of  $n_k^x$ , parallel to the drive, and indeed matches our observations. Second, in theory, the inverse particle flux also results in a delayed counter-propagating ‘reflected’ flux [28, 30], which is formally required for the steady state to be established [45]. We do not observe this flux directly for isotropic driving, but here it is revealed perpendicular to the drive, where there is no inverse flux (see bottom cartoon): the  $n_k^y$  populations do grow, but only with a delay, after the growth of  $n_k^x$  (for  $k \gtrsim k_\xi$ ) is nearly complete. At long times,  $n_k^y$  is approximately  $\propto k^{-2.4}$  (see [41]), but we are not aware of any prediction for this purely reflected cascade.

In conclusion, our experiments demonstrate an inverse turbulent-wave cascade in a driven 2D Bose gas, and we also qualitatively confirm the main expectations for its formation dynamics. In the future, it would be interesting to measure the underlying cascade fluxes [34] and test the expected self-similar evolution at pre-steady-state times [29, 30]. Such studies would greatly benefit from an extension of the cascade

spectral range (here limited by our optical resolution [41]), which could be increased by an order of magnitude using an optical lattice to drive the gas, capitalizing on our observation that uniaxial driving preserves the key features of the cascade. At low  $k$ , the stationary nonthermal spectrum we observe has a characteristic lengthscale  $(1/k_0)$ , whose origin could be linked to the recently proposed concept of emergent lengthscales in nonlinear driven systems [46].

We thank Panagiotis Christodoulou and Nishant Dogra for early contributions and Gevorg Martirosyan, Jiří Etrych, Jürgen Berges, and Aleksas Mazeliauskas for discussions and comments on the manuscript. This work was supported by EPSRC [Grant No. EP/P009565/1], ERC (UniFlat), and STFC [Grant No. ST/T006056/1]. M. Gałka acknowledges support from Germany’s Excellence Strategy EXC2181/1-390900948 (Heidelberg Excellence Cluster STRUCTURES). Z.H. acknowledges support from the Royal Society Wolfson Fellowship.

- 
- [1] L. F. Richardson, *Weather prediction by numerical process* (Cambridge University Press, 1922).
  - [2] A. N. Kolmogorov, The local structure of turbulence in incompressible viscous fluid for very large Reynolds numbers, *Dokl. Akad. Nauk SSSR* **30**, 299 (1941).
  - [3] A. Obukhov, On the distribution of energy in the spectrum of turbulent flow, *Dokl. Akad. Nauk SSSR* **32**, 22 (1941).
  - [4] L. Sorriso-Valvo, R. Marino, V. Carbone, A. Noullez, F. Lepreti, P. Veltri, R. Bruno, B. Bavassano, and E. Pietropaolo, Observation of Inertial Energy Cascade in Interplanetary Space Plasma, *Phys. Rev. Lett.* **99**, 115001 (2007).
  - [5] S. Ghoshghaie, W. Breymann, J. Peinke, P. Talkner, and Y. Dodge, Turbulent cascades in foreign exchange markets, *Nature* **381**, 767 (1996).
  - [6] R. H. Kraichnan, Inertial Ranges in Two-dimensional Turbu-

- lence, *Phys. Fluids* **10**, 1417 (1967).
- [7] J. Paret and P. Tabeling, Experimental Observation of the Two-Dimensional Inverse Energy Cascade, *Phys. Rev. Lett.* **79**, 4162 (1997).
- [8] M. A. Rutgers, Forced 2D Turbulence: Experimental Evidence of Simultaneous Inverse Energy and Forward Enstrophy Cascades, *Phys. Rev. Lett.* **81**, 2244 (1998).
- [9] R. M. B. Young and P. L. Read, Forward and inverse kinetic energy cascades in Jupiter's turbulent weather layer, *Nat. Phys.* **13**, 1135 (2017).
- [10] G. Gauthier, M. T. Reeves, X. Yu, A. S. Bradley, M. A. Baker, T. A. Bell, H. Rubinsztein-Dunlop, M. J. Davis, and T. W. Neely, Giant vortex clusters in a two-dimensional quantum fluid, *Science* **364**, 1264 (2019).
- [11] S. P. Johnstone, A. J. Groszek, P. T. Starkey, C. J. Billington, T. P. Simula, and K. Helmerston, Evolution of large-scale flow from turbulence in a two-dimensional superfluid, *Science* **364**, 1267 (2019).
- [12] R. Panico, P. Comaron, M. Matuszewski, A. S. Lanotte, D. Trypogeorgos, G. Gigli, M. D. Giorgi, V. Ardizzone, D. Sanvitto, and D. Ballarini, Onset of vortex clustering and inverse energy cascade in dissipative quantum fluids, *Nat. Photon.* **17**, 451 (2023).
- [13] S. Galtier and S. V. Nazarenko, Turbulence of Weak Gravitational Waves in the Early Universe, *Phys. Rev. Lett.* **119**, 221101 (2017).
- [14] S. Galtier, S. V. Nazarenko, Éric Buchlin, and S. Thalabard, Nonlinear diffusion models for gravitational wave turbulence, *Phys. D: Nonlinear Phenom.* **390**, 84 (2019).
- [15] D. Biskamp, E. Schwarz, and J. F. Drake, Two-Dimensional Electron Magnetohydrodynamic Turbulence, *Phys. Rev. Lett.* **76**, 1264 (1996).
- [16] A. Brandenburg, Hall cascade with fractional magnetic helicity in neutron star crusts, *Astrophys. J.* **901**, 18 (2020).
- [17] U. Bortolozzo, J. Laurie, S. Nazarenko, and S. Residori, Optical wave turbulence and the condensation of light, *J. Opt. Soc. Am. B* **26**, 2280 (2009).
- [18] J. Laurie, U. Bortolozzo, S. Nazarenko, and S. Residori, One-dimensional optical wave turbulence: Experiment and theory, *Phys. Rep.* **514**, 121 (2012).
- [19] D. Pierangeli, F. Di Mei, G. Di Domenico, A. J. Agranat, C. Conti, and E. DelRe, Turbulent Transitions in Optical Wave Propagation, *Phys. Rev. Lett.* **117**, 183902 (2016).
- [20] E. Falcon, G. Michel, G. Prabhudesai, A. Cazaubiel, M. Berhanu, N. Mordant, S. Aumaître, and F. Bonnefoy, Saturation of the Inverse Cascade in Surface Gravity-Wave Turbulence, *Phys. Rev. Lett.* **125**, 134501 (2020).
- [21] L. Chomaz, L. Corman, T. Bienaimé, R. Desbuquois, C. Weitenberg, S. Nascimbène, J. Beugnon, and J. Dalibard, Emergence of coherence via transverse condensation in a uniform quasi-two-dimensional Bose gas, *Nat. Commun.* **6**, 6162 (2015).
- [22] N. Navon, R. P. Smith, and Z. Hadzibabic, Quantum gases in optical boxes, *Nat. Phys.* **17**, 1334 (2021).
- [23] S. Dyachenko, A. C. Newell, A. Pushkarev, and V. E. Zakharov, Optical turbulence: weak turbulence, condensates and collapsing filaments in the nonlinear Schrödinger equation, *Phys. D: Nonlinear Phenom.* **57**, 96 (1992).
- [24] J. Berges, A. Rothkopf, and J. Schmidt, Nonthermal Fixed Points: Effective Weak Coupling for Strongly Correlated Systems Far from Equilibrium, *Phys. Rev. Lett.* **101**, 041603 (2008).
- [25] I. Chantesana, A. Piñeiro Orioli, and T. Gasenzer, Kinetic theory of nonthermal fixed points in a Bose gas, *Phys. Rev. A* **99**, 043620 (2019).
- [26] M. Gazo, A. Karailiev, T. Satoor, C. Eigen, M. Gałka, and Z. Hadzibabic, Universal Coarsening in a Homogeneous Two-Dimensional Bose Gas, [arXiv:2312.09248](https://arxiv.org/abs/2312.09248) (2023).
- [27] D. V. Semikoz and I. I. Tkachev, Kinetics of Bose Condensation, *Phys. Rev. Lett.* **74**, 3093 (1995).
- [28] S. Galtier, S. V. Nazarenko, A. C. Newell, and A. Pouquet, A weak turbulence theory for incompressible magnetohydrodynamics, *J. Plasma Phys.* **63**, 447 (2000).
- [29] B. Semisalov, V. Grebenev, S. Medvedev, and S. Nazarenko, Numerical analysis of a self-similar turbulent flow in Bose-Einstein condensates, *Commun. Nonlinear Sci. Numer. Simul.* **102**, 105903 (2021).
- [30] Y. Zhu, B. Semisalov, G. Krstulovic, and S. Nazarenko, Self-similar evolution of wave turbulence in Gross-Pitaevskii system, *Phys. Rev. E* **108**, 064207 (2023).
- [31] P. Christodoulou, M. Gałka, N. Dogra, R. Lopes, J. Schmitt, and Z. Hadzibabic, Observation of first and second sound in a BKT superfluid, *Nature* **594**, 191 (2021).
- [32] J. Etrych, G. Martirosyan, A. Cao, J. A. P. Glidden, L. H. Dogra, J. M. Hutson, Z. Hadzibabic, and C. Eigen, Pinpointing Feshbach resonances and testing Efimov universalities in  $^{39}\text{K}$ , *Phys. Rev. Res.* **5**, 013174 (2023).
- [33] Z. Hadzibabic and J. Dalibard, Two-dimensional Bose fluids: An atomic physics perspective, *Riv. del Nuovo Cim.* **34**, 389 (2011).
- [34] N. Navon, C. Eigen, J. Zhang, R. Lopes, A. L. Gaunt, K. Fujimoto, M. Tsubota, R. P. Smith, and Z. Hadzibabic, Synthetic dissipation and cascade fluxes in a turbulent quantum gas, *Science* **366**, 382 (2019).
- [35] S. Tung, G. Lamporesi, D. Lobser, L. Xia, and E. A. Cornell, Observation of the Presuperfluid Regime in a Two-Dimensional Bose Gas, *Phys. Rev. Lett.* **105**, 230408 (2010).
- [36] S. Nazarenko and M. Onorato, Wave turbulence and vortices in Bose-Einstein condensation, *Phys. D: Nonlinear Phenom.* **219**, 1 (2006).
- [37] S. Nazarenko, *Wave Turbulence* (Springer, 2011).
- [38] Y. Zhu, B. Semisalov, G. Krstulovic, and S. Nazarenko, Direct and Inverse Cascades in Turbulent Bose-Einstein Condensates, *Phys. Rev. Lett.* **130**, 133001 (2023).
- [39] G. Gauthier, I. Lenton, N. M. Parry, M. Baker, M. J. Davis, H. Rubinsztein-Dunlop, and T. W. Neely, Direct imaging of a digital-micromirror device for configurable microscopic optical potentials, *Optica* **3**, 1136 (2016).
- [40] Y.-Q. Zou, E. L. Cerf, B. Bakkali-Hassani, C. Maury, G. Chauveau, P. C. M. Castilho, R. Saint-Jalm, S. Nascimbene, J. Dalibard, and J. Beugnon, Optical control of the density and spin spatial profiles of a planar Bose gas, *J. Phys. B: At. Mol. Opt. Phys.* **54**, 08LT01 (2021).
- [41] See Supplemental Material for details of the DMD driving and an additional panel for Fig. 5.
- [42] For our strong drive, we observe efficient excitation over about  $\pm 120$  Hz from our drive frequency.
- [43] M. Gałka, P. Christodoulou, M. Gazo, A. Karailiev, N. Dogra, J. Schmitt, and Z. Hadzibabic, Emergence of Isotropy and Dynamic Scaling in 2D Wave Turbulence in a Homogeneous Bose Gas, *Phys. Rev. Lett.* **129**, 190402 (2022).
- [44] The particle recirculation would be perfect in the limit  $k_D/k_F \rightarrow \infty$ , in which the direct cascade would not carry away any particles. In our case, the normalized  $n_k$  is stationary.
- [45] The necessity of the reflected flux is due to the fact that the inverse cascade has a finite particle capacity; in contrast, the direct cascade has an infinite energy capacity [37].
- [46] X. M. de Wit, M. Fruchart, T. Khain, F. Toschi, and V. Vitelli, Pattern formation by turbulent cascades, *Nature* **627**, 515 (2024).



## SUPPLEMENTAL MATERIAL

## DMD driving

We use DMD grayscaleing to create our time-varying drive potentials. Our imaging resolution is approximately  $1.5\text{ }\mu\text{m}$ , whereas a DMD pixel corresponds to  $0.22\text{ }\mu\text{m}$  in the atomic plane, which gives  $(1.5/0.22)^2 \approx 46$  grayscale levels [39, 40]. As in [40], we use an error diffusion algorithm to convert continuous functions into binary masks. Our imaging resolution also sets the smallest achievable forcing lengthscale, which in momentum space corresponds to  $k_F \approx 2.1\text{ }\mu\text{m}^{-1}$ .

For the circular trap (with radius  $R = 22\text{ }\mu\text{m}$ ) used for Figs. 2-4, radially-symmetric excitation modes have the form  $J_0(q_n r/R)$ , where  $J_0(r)$  is the zeroth-order Bessel function of the first kind, and  $q_n$  corresponds to its  $n^{\text{th}}$  extremum. For the square trap (with side length  $L = 30\text{ }\mu\text{m}$ ) used for Fig. 5, we excite a mode of the form  $\cos(n\pi(x+L/2)/L)$ . Our potentials for the circular and square traps correspond, respectively, to  $n = 14$  and  $n = 21$ .

## Additional panel for Fig. 5

The uniaxial driving protocol used for Fig. 5 results in anisotropic momentum distributions at long drive times. In Fig. S1 we show  $n_k^y$  for the same times as in Fig. 5(b). The black line corresponds to  $n_k^y \propto k^{-2.4}$ .

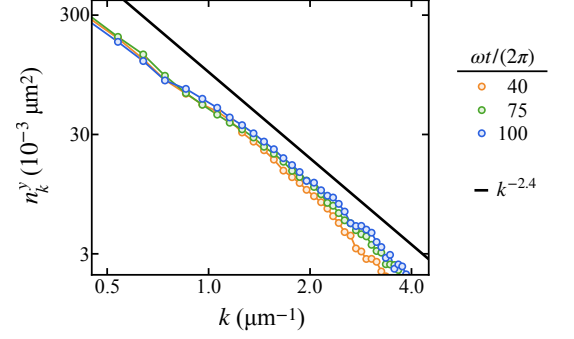


FIG. S1. Momentum distributions  $n_k^y$ , perpendicular to the uniaxial drive. The black line corresponds to  $n_k^y \propto k^{-2.4}$ .